Proceeding Paper

Effects of Guanidinium Addition to CH₃NH₃PbI₃ Perovskite Solar Cells Inserted with Decaphenylpentasilane †

Iori Ono [1],*, **Takeo Oku** [1],*, **Atsushi Suzuki** [1], **Masanobu Okita** [2], **Sakiko Fukunishi** [2], **Tomoharu Tachikawa** [2] **and Tomoya Hasegawa** [2]

1 Department of Materials Science, The University of Shiga Prefecture, 2500 Hassaka, Hikone 522-8533, Japan; suzuki@mat.usp.ac.jp

2 Osaka Gas Chemicals Co., Ltd., 5-11-61 Torishima, Konohana-ku, Osaka 554-0051, Japan; okita@ogc.co.jp (M.O.); fukunishi@ogc.co.jp (S.F.); t-tachikawa@ogc.co.jp (T.T.); hasegawa_tomoya@ogc.co.jp (T.H.)

* Correspondence: ov21ishimaji@ec.usp.ac.jp (I.O.); oku@mat.usp.ac.jp (T.O.); Tel.: +81-749-28-8368 (T.O.)

† Presented at the 3rd International Electronic Conference on Crystals, 15–30 January 2022; Available online: https://iocc_2022.sciforum.net/.

Abstract: Effects of addition of guanidinium [C(NH₂)₃; GA] on MAPbI₃ perovskite solar cells fabricated at a high temperature of 190 °C in atmospheric air were investigated on the photovoltaic properties and first principles calculations. The addition of guanidinium iodide and the insertion of decaphenylpentasilane between the perovskite and hole transport layer improved the external quantum efficiency and short-circuit current density, and the conversion efficiencies were stable after 1 month. First principles calculations on the density of states and band structures showed reduction of the total energy by the GA addition and the effectiveness of the nitrogen atoms in GA.

Keywords: perovskite; solar cell; methylammonium; guanidinium; polysilane; first principles calculation

1. Introduction

The most common solar cells are currently silicon solar cells. However, the silicon solar cells have a complicated fabrication process and are expensive. Recently developed CH₃NH₃PbI₃ (MAPbI₃)-based perovskite compounds have demonstrated numerous advantages, such as tunable band gaps, easy fabrication process, and high conversion efficiencies [1–5]. Higher efficiencies have been accomplished for various perovskite compounds and device structures, and conversion efficiencies above 20% have been achieved [6–14]. However, MAPbI₃ perovskite compounds are typically unstable in air because of the migration of CH₃NH₃ (MA). Therefore, the stability of the corresponding perovskite solar cells should be improved for inclusion in the actual cell module [15]. One method to improve the stability of perovskite solar cells is elemental or molecular adding to the perovskite crystals [16–23].

As guanidinium (C(NH₂)₃, GA) have larger ionic radii (2.78 Å) than MA (2.17 Å), which can be expected to improve the structural stability. Several studies on GA addition have been carried out, and the photovoltaic properties and stability of the MAPbI₃ were improved [24–27]. GA addition is expected to extend the carrier lifetime and to reduce the carrier recombination in the perovskite layers [28,29]. In addition to the GA addition, various organic and alkali cations such as formamidinium (CH(NH₂)₂, FA) [30,31], ethyl ammonium (CH₃CH₂NH₂, EA) [32,33], cesium (Cs) [31,34], rubidium (Rb) [35,36], potassium (K) [21,37], or sodium (Na) [20] were added to stabilize the MAPbI₃ perovskite crystals, and the photovoltaic properties were improved by these additions.

Incorporating polymeric materials into the perovskite devices is another approach to improve the stability of perovskite solar cells [38]. For example, coating a thin layer of poly(methyl methacrylate) on top of the perovskite layer forms a cross-linked network

structure, which protects the cell from moisture and oxygen [39]. Polysilanes have two important features. First, polysilanes are p-type semiconductors, which promote hole transfer [40]. Second, polysilanes are more stable at elevated temperatures above 300 °C than ordinary organic materials, which is expected as a protective layer when deposited on perovskite compounds. Therefore, polysilanes, such as decaphenylcyclopentasilane (DPPS), have been applied as HTLs of MAPbI$_3$ perovskite devices [41,42].

The purpose of the present work is to fabricate and characterize perovskite solar cells in which a small amount of GA was added to MAPbI$_3$, and annealed at high temperature of 190 °C in ambient air applying the DPPS layer on the perovskite layer. These experimental results were also compared with calculated electronic states and band structures. PbCl$_2$ and CH$_3$NH$_3$PbI$_3$ were selected to form the perovskite crystals based on the following chemical equation: CH$_3$NH$_3$I + PbCl$_2$ = 2CH$_3$NH$_3$Cl + MAPbI$_3$. The annealing temperature is higher than 140 °C, which may lead the stabilization of the perovskite grains [43]. A small amount of chlorine could improve the diffusion length of excitons and the carrier lifetime, which improved the conversion efficiency [44,45].

Effects of GA adding to MAPbI$_3$ crystals on the electronic structures were also investigated by first-principles calculation. The effects of GA addition on the microstructures and photovoltaic properties of the MAPbI$_3$ perovskite solar cells were investigated using current density-voltage (*J-V*) characteristics, X-ray diffraction (XRD).

2. Experimental Procedures

A method for fabricating a perovskite solar cell is shown in Figure 1. Details were described in the previous works [46–50]. F-doped tin-oxide (FTO) substrates were cleaned by using an ultrasonic bath with acetone and methanol, and dried under nitrogen. TiO$_2$ precursor solutions (0.15 and 0.30 M compact TiO$_2$) were prepared from titanium diisopropoxide bis(acetylacetonate) (Sigma-Aldrich, Tokyo, Japan, 0.055 and 0.11 mL) with 1-butanol (Nacalai Tesque, 1 mL), and the 0.15 M TiO$_2$ precursor solution was spin-coated on the FTO substrate at 3000 rpm for 30 s and annealed at 125 °C for 5 min in air to form the compact TiO$_2$ layer. Mesoporous TiO$_2$ precursor solution was spin-coated on the compact TiO$_2$ at 5000 rpm for 30 s and annealed at 550 °C for 30 min in air to form the mesoporous TiO$_2$ layer.
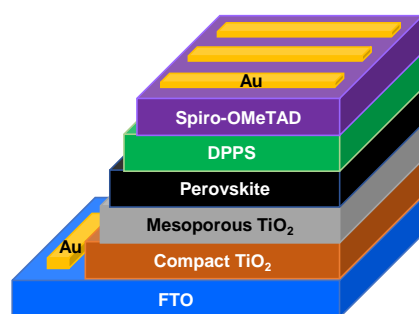

Figure 1. Schematic illustration of the perovskite solar cells.

The perovskite compounds were prepared with N-dimethylformamide (Sigma-Aldrich) of mixing CH$_3$NH$_3$I (Tokyo Chemical Industry, Tokyo, Japan, 190.8 mg) and PbCl$_2$ (Sigma-Aldrich, 111.2 mg) at 60 °C for 24 h. This solution was the basic precursor of MAPbI$_3$, prepared with a mole ratio of 3:1 [43]. MA$_{0.9}$GA$_{0.1}$PbI$_3$ and MA$_{0.8}$GA$_{0.2}$PbI$_3$ precursors were prepared by adding guanidinium iodide (Sigma Aldrich) to control the desired molar ratio. Perovskite precursor solutions were spin-coated on the mesoporous TiO$_2$ layer three times applying a hot air blowing method during the spin-coatings. The perovskite solutions were spin-coated at 2000 rpm for 60 s. On the third spin-coating, decaphenyl-cyclopentasilane (DPPS, Osaka Gas Chemicals, Osaka, Japan, SI-30-15, 10 mg) solution were dropped on the perovskite layer [42,51,52]. The polysilane solution was prepared by mixing chlorobenzene (Fujifilm Wako Pure Chemical Corporation, Osaka, Japan, 0.5 mL)

with DPPS. After the spin-coating, the prepared cells were annealed at 190 °C for 10 min in air to form the perovskite layer.

A hole transport layer was prepared by spin-coating on the perovskite layer. A precursor solution of the hole transport layer was prepared by mixing chlorobenzene and 2,2′,7,7′-tetrakis-(N,N-di(p-methoxyphenyl)amine)-9,9′-spirobifluorene (Sigma Aldrich, spiro-OMeTAD) for 12 h. This solution was added that mixing an acetonitrile (Nacalai Tesque, Kyoto, Japan, 0.5 mL) with 4-tert-butylpyridine (Sigma-Aldrich, 188 mg) and lithium bis(trifluoromethylsulfonyl)imide (Tokyo Chemical Industry, 260 mg), stirred at 70 °C for 30 min. Finally, a gold (Au) thin films was evaporated onto the hole transport layer, as top metal electrodes.

The current density voltage characteristics (Keysight, Santa Rosa, CA, USA, B2901A) of the fabricated devices were measured under a solar simulating light source (San-ei Electric, Osaka, Japan, XES-301S) operated at 100 mW cm^{-2}. X-ray diffraction (XRD, Bruker, Billerica, MA, USA, D2 PHASER) was used to investigate the microstructures of the devices.

3. Result and Discussion

Measured photovoltaic parameters are shown in Table 1. The standard cell provided a short-circuit current density (J_{SC}) of 19.2 mA cm^{-2} and a conversion efficiency (η) of 11.95%. The addition of 10% GA increased J_{SC} to 21.5 mA cm^{-2} from 19.2 mA cm^{-2}, η to 13.88% from 11.95. The η was improved by the GA addition because of a proportional relationship between J_{SC} and η. The highest J_{SC} and open-circuit voltage (V_{OC}) were obtained for the addition of 10% GA, which provided an η_{ave} of 13.16%. The average efficiency (η_{ave}) of three electrodes was measured. After one month, the η values for the standard and +GAI cells were stable.

Table 1. Measured photovoltaic parameters of solar cells.

Device	J_{SC} (mA cm^{-2})	V_{OC} (V)	FF	R_S (Ω cm^{-2})	R_{sh} (Ω cm^{-2})	η (%)	η_{ave} (%)	E_g (eV)	η_{ave} (After 1 Month) (%)
Standard	19.2	0.819	0.760	4.78	635	11.95	11.74	1.546	11.01
GA 10%	21.5	0.835	0.773	4.66	633	13.88	13.16	1.533	12.36
GA 20%	21.2	0.793	0.634	7.64	238	10.68	9.84	1.547	9.77

Calculated electronic structures of the MAPbI$_3$, MA$_{0.875}$GA$_{0.125}$PbI$_3$, and MA$_{0.75}$GA$_{0.25}$PbI$_3$ at the highest occupied molecular orbital (HOMO), the lowest unoccupied molecular orbital (LUMO) energy levels and the electrostatic potential map are shown in Figure 2, which were calculated by *ab-initio* methods based on the Hartree–Fock [53–59]. The phases of electron densities in the Pb-6p and I-5p orbitals were inverted, as indicated by the green and red coloration. Since the constructed supercell models are MA$_7$GAPb$_8$I$_{24}$ and MA$_6$GA$_2$Pb$_8$I$_{24}$, the chemical compositions are denoted as MA$_{0.875}$GA$_{0.125}$PbI$_3$ and MA$_{0.75}$GA$_{0.25}$PbI$_3$, respectively. Although the compositions are not precisely same as those of GA10% and GA 20% crystals, some tendencies on the properties of the crystals could be estimated. The electronic charge of the LUMO showed that the electron would flow straight. The electronic charge of the HOMO was distributed over the nitrogen of in the GA, which contributed to the carrier transport and electronic properties. The electrostatic potential was positive (blue) around the methylammonium and guanidinium. Partial density of states (DOS) of the MAPbI$_3$, MA$_{0.875}$GA$_{0.125}$PbI$_3$, and MA$_{0.75}$GA$_{0.25}$PbI$_3$ perovskite crystals are shown in Figure 3. The electrons were increased at −2 eV with the GA addition.
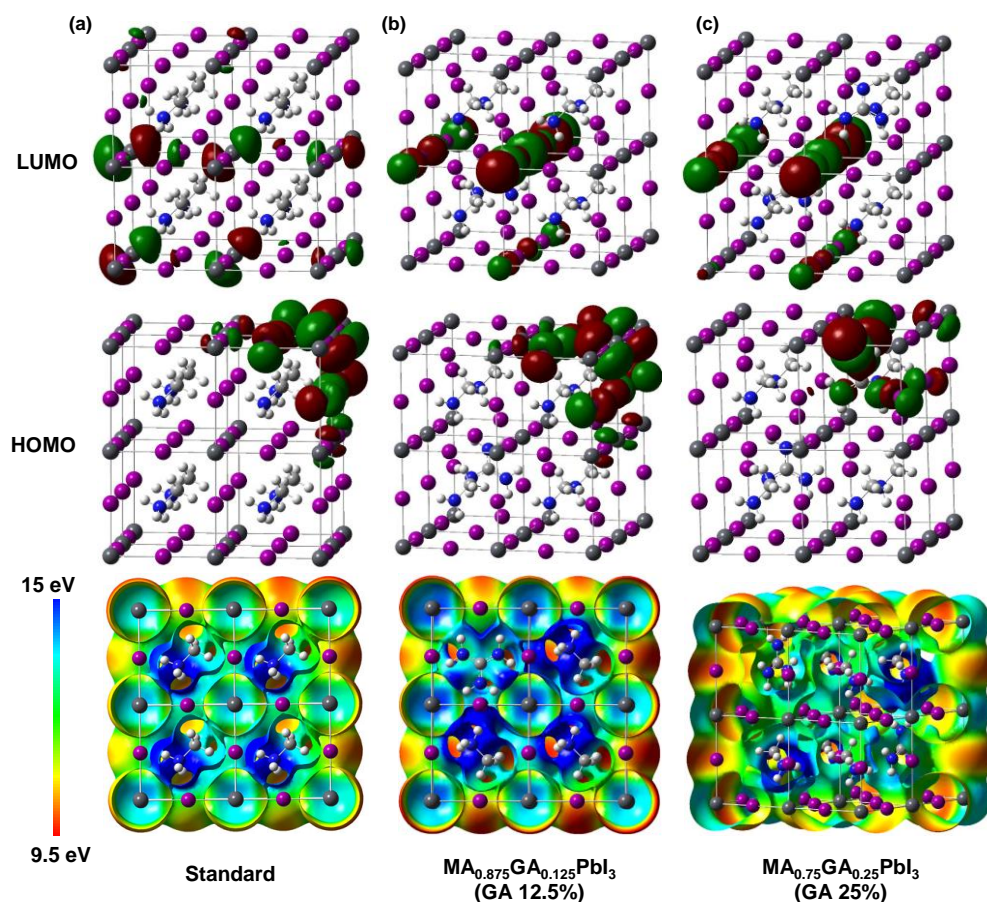
Figure 2. LUMO, HOMO, and cutaway view of electrostatic potential for (**a**) MAPbI$_3$, (**b**) MA$_{0.875}$GA$_{0.125}$PbI$_3$, and (**c**) MA$_{0.75}$GA$_{0.25}$PbI$_3$.
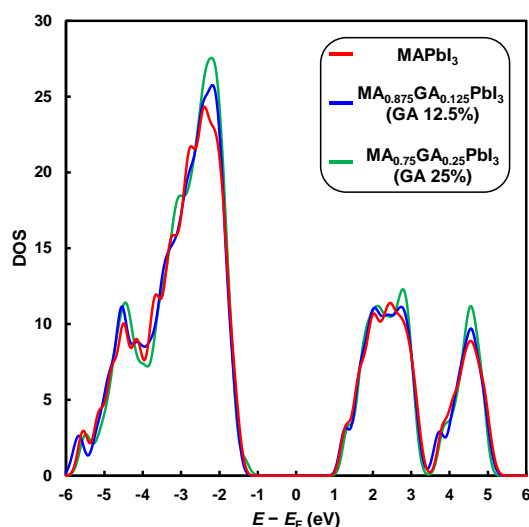
Figure 3. DOS of MAPbI$_3$, MA$_{0.875}$GA$_{0.125}$PbI$_3$, MA$_{0.75}$GA$_{0.25}$PbI$_3$.

Table 2 shows energy levels of MAPbI$_3$, MA$_{0.875}$GA$_{0.125}$PbI$_3$ and MA$_{0.75}$GA$_{0.25}$PbI$_3$ from the calculation. MAPbI$_3$ provided a HOMO of -17.78 eV, a LUMO-15.00 eV, Fermi level (E_F) of -16.39 eV, band gap (E_g) of 1.02 eV. The E_g increased from 1.02 to 0.93 eV by the GA, which may increase the J_{SC} and η. Gibbs energy (G) decreased for structure models by adding GA, which indicates the perovskite crystals are stabilized by the addition of GA.

Table 2. Energy levels of MAPbI$_3$, MA$_{0.875}$GA$_{0.125}$PbI$_3$ and MA$_{0.75}$GA$_{0.25}$PbI$_3$ calculated by molecular orbital calculation.

Structure	HOMO (eV)	LUMO (eV)	E_F (eV)	E_g (eV)	G (kJ mol^{-1})
MAPbI$_3$	−17.78	−15.00	−16.39	1.02	−1470
MA$_{0.875}$GA$_{0.175}$PbI$_3$	−17.81	−15.02	−16.42	1.02	−1578
MA$_{0.75}$GA$_{0.25}$PbI$_3$	−17.63	−14.94	−16.28	0.93	−1686

Lattice constants of standard, GA10% and GA20% perovskites were measured to be 6.268 Å, 6.276 Å and 6.278 Å, respectively, which indicates an increase by the GA addition. Since the ionic radius of GA$^+$ is larger than MA$^+$, the increase in the lattice constant would be due to the substitution of GA at the MA-site [60].

The band structures and partial DOS of the MAPbI$_3$, MA$_{0.875}$GA$_{0.125}$PbI$_3$ and MA$_{0.75}$GA$_{0.25}$PbI$_3$ perovskite crystals were calculated by first-principles calculation [59], as shown in Figure 4. Figure 4 shows the 6p orbital of Pb is widely distributed near the conduction band minimum for both crystals. Near the valence band maximum, the 5p orbital of I and the 6s orbital of Pb are distributed. For the MA$_{0.875}$GA$_{0.125}$PbI$_3$, the 2p orbital of nitrogen in the GA is distributed at −2 eV, which could promote the improvement of the current density.
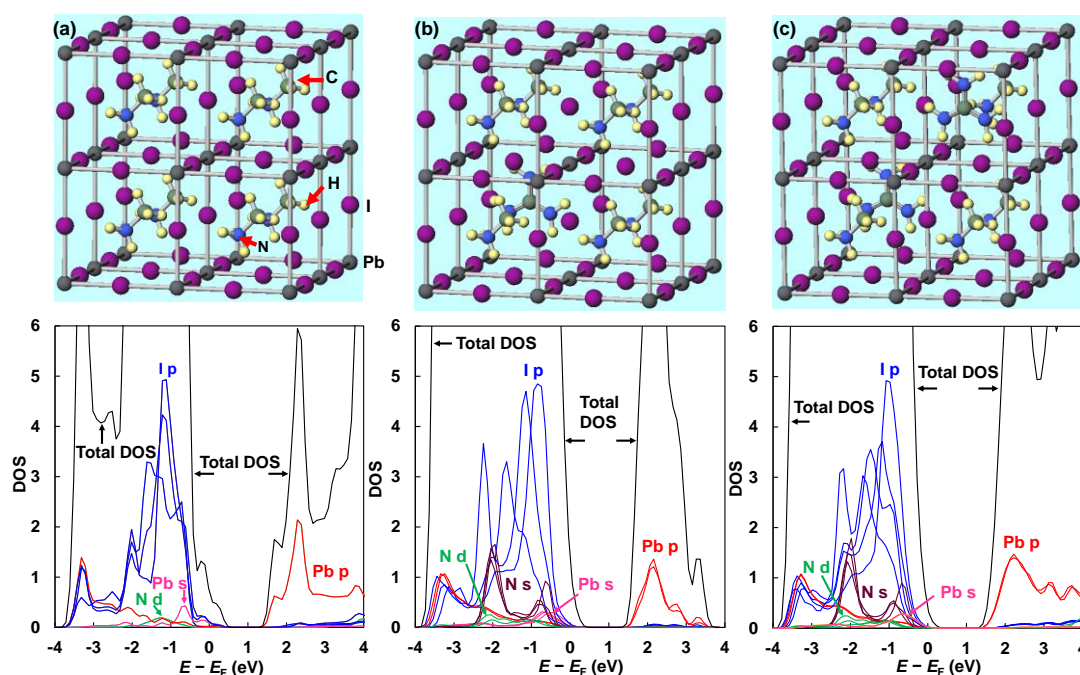
Figure 4. Structure models, density of states, and band structures for (**a**) MAPbI$_3$ and (**b**) MA$_{0.875}$GA$_{0.125}$PbI$_3$ and (**c**) MA$_{0.75}$GA$_{0.25}$PbI$_3$.

Electron density distributions of MA$_{0.875}$GA$_{0.125}$PbI$_3$ are shown in Figure 5. The electron density distributions around MA and GA are positively charged. The electron density distribution around GA was slightly lower than that around MA on the Pb-I interfaces, which indicates that carriers around GA would flow and stabilize the perovskite crystals. Table 3 shows the bandgap and total energy of the perovskite crystal lattice obtained from the calculation. The bandgap energies of MAPbI$_3$ and MA$_{0.875}$GA$_{0.125}$PbI$_3$ are calculated to be 1.33 eV and 1.31 eV, respectively. Calculated results on the total energies indicate the GA addition promotes stabilization of the perovskite crystal, which is expected to suppress the desorption of MA or GA. The GA addition also causes a reduction in the bandgap and increases the number of excited electrons.
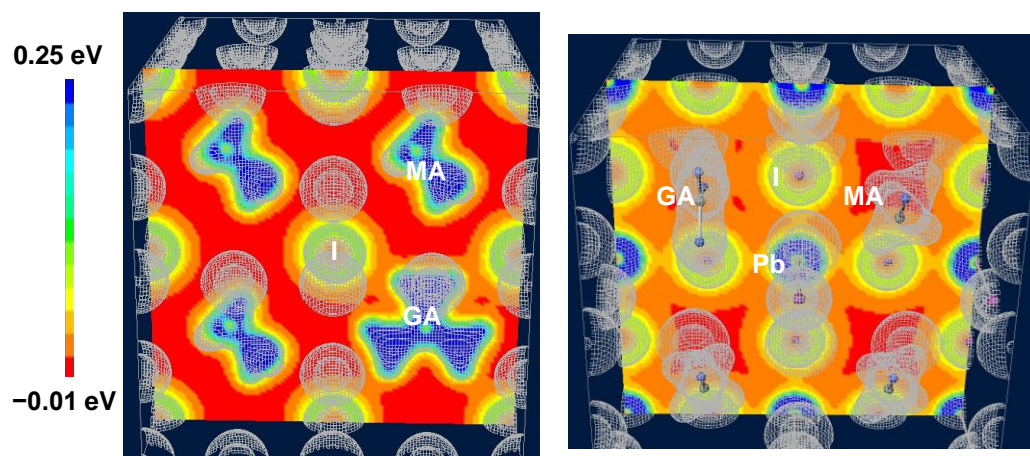
Figure 5. Electron density distribution of $MA_{0.875}GA_{0.125}PbI_3$.

Table 3. Band gap and total energies of $MAPbI_3$, $MA_{0.875}GA_{0.125}PbI_3$ and $MA_{0.75}GA_{0.25}PbI_3$ by band calculation.

Structure Model	Band Gap (eV)	Total Energy (eV cell^{-1})
$MAPbI_3$	1.326	−3496
$MA_{0.875}GA_{0.175}PbI_3$	1.305	−3629
$MA_{0.75}GA_{0.25}PbI_3$	1.313	−3629

4. Conclusions

EQE and J_{SC} were improved by the GA addition to the $MAPbI_3$. The η of 12% was maintained for the GA10% added device even after 1 month. The synergistic effect of the addition of GA and insertion of polysilane for the high temperature fabrication of solar cells is effective for stabilization of perovskite solar cells. From the results of first-principles calculations, the carrier transport was changed by the GA addition.

Author Contributions: Conceptualization, I.O. and T.O.; Methodology, I.O., T.O. and A.S.; Formal Analysis, I.O., T.O. and A.S.; Investigation, I.O., T.O. and A.S.; Resources, M.O., S.F., T.T. and T.H.; Data Curation, I.O. and T.O.; Writing—Original Draft Preparation, I.O. and T.O.; Writing—Review & Editing, I.O., T.O., A.S., M.O., S.F., T.T. and T.H.; Project Administration, T.O.; Funding Acquisition, T.O. All authors have read and agreed to the published version of the manuscript.

Institutional Review Board Statement: Not applicable.

Informed Consent Statement: Not applicable.

Data Availability Statement: Data is contained within the article.

Conflicts of Interest: The authors declare no conflict of interest.

References

1. Kojima, A.; Teshima, K.; Shirai, Y.; Miyasaka, T. Organometal halide perovskites as visible-light sensitizers for photovoltaic cells. *J. Am. Chem. Soc.* **2019**, *131*, 6050. [CrossRef] [PubMed]
2. Kim, H.-S.; Lee, C.-R.; Im, J.-H.; Lee, K.-B.; Moehl, T.; Marchioro, A.; Moon, S.-J.; Yum, J.-H.; Humphry-Baker, R.; Moser, J.E.; et al. Lead iodide perovskite sensitized all-solid-state submicron thin film mesoscopic solar cell with efficiency exceeding 9%. *Sci. Rep.* **2012**, *2*, 591. [CrossRef] [PubMed]
3. Li, N.; Zhu, Z.; Chueh, C.-C.; Liu, H.; Peng, B.; Petrone, A.; Li, X.; Wang, L.; Jen, K.-Y.A. Mixed cation $FA_xPEA_{1-x}PbI_3$ with enhanced phase and ambient stability toward high-performance perovskite solar cells. *Adv. Energy Mater.* **2017**, *7*, 1601307. [CrossRef]
4. Gedamu, D.; Asuo, M.I.; Benetti, D.; Basti, M.; Ka, I.; Cloutier, G.S.; Rosei, F.; Nechache, R. solvent-antisolvent ambient processed large grain size perovskite thin films for high-performance solar cells. *Sci. Rep.* **2018**, *8*, 12885. [CrossRef] [PubMed]

5. Tong, J.; Song, Z.; Kim, H.D.; Chen, X.; Chen, C.; Palmstrom, A.; Ndione, F.P.; Reese, O.M.; Dunfield, P.S.; Zhu, K.; et al. Carrier lifetimes of >1 μs in Sn-Pb perovskites enable efficient all-perovskite tandem solar cells. *Science* **2019**, *364*, 475. [CrossRef] [PubMed]

6. Saliba, M.; Orlandi, S.; Matsui, T.; Aghazada, S.; Cavazzini, M.; Correa-Baena, J.-P.; Gao, P.; Scopelliti, R.; Mosconi, E.; Dahmen, K.-H.; et al. A molecularly engineered hole-transporting material for efficient perovskite solar cells. *Nat. Energy* **2016**, *1*, 15017. [CrossRef]

7. Bi, D.; Yi, C.; Luo, J.; Decoppet, J.-D.; Zhang, F.; Zakeeruddin, M.S.; Li, X.; Hagfeldt, A.; Gratzel, M. Polymer-templated nucleation and crystal growth of perovskite films for solar cells with efficiency greater than 21%. *Nat. Energy* **2016**, *1*, 16142. [CrossRef]

8. Saliba, M.; Matsui, T.; Domanski, K.; Seo, J.-Y.; Ummadisingu, A.; Zakeeruddin, M.S.; Correa-Baena, J.-P.; Tress, R.W.; Abate, A.; Hagfeldt, A.; et al. Incorporation of rubidium cations into perovskite solar cells improves photovoltaic performance. *Science* **2016**, *354*, 206. [CrossRef]

9. He, M.; Li, B.; Cui, X.; Jiang, B.; He, Y.; Chen, Y.; O'Neil, D.; Szymanski, P.; El-Sayed, A.M.; Huang, J.; et al. Meniscus-assisted solution printing of large-grained perovskite films for high-efficiency solar cells. *Nat. Commun.* **2017**, *8*, 16045. [CrossRef]

10. Jeon, J.N.; Na, H.; Jung, H.E.; Yang, T.-Y.; Lee, G.Y.; Kim, G.; Shin, H.-W.; Seok, I.S.; Lee, J.; Seo, J. A fluorene-terminated hole-transporting material for highly efficient and stable perovskite solar cells. *Nat. Energy* **2018**, *3*, 682. [CrossRef]

11. Kim, G.; Min, H.; Lee, S.K.; Lee, Y.D.; Yoon, M.S.; Seok, I.S. Impact of strain relaxation on performance of α-formamidinium lead iodide perovskite solar cells. *Science* **2020**, *370*, 108. [CrossRef] [PubMed]

12. Yoo, J.J.; Seo, G.; Chua, R.M.; Park, G.T.; Lu, Y.; Rotermund, F.; Kim, Y.-K.; Moon, S.C.; Jeon, J.N.; Correa-Baena, J.-P.; et al. Efficient perovskite solar cells via improved carrier management. *Nature* **2021**, *590*, 587. [CrossRef] [PubMed]

13. Hui, W.; Chao, L.; Lu, H.; Xia, F.; Wei, Q.; Su, Z.; Niu, T.; Tao, L.; Du, B.; Huang, W.; et al. Stabilizing black-phase formamidinium perovskite formation at room temperature and high humidity. *Science* **2021**, *371*, 1359. [CrossRef] [PubMed]

14. Madan, J.; Singh, K.; Pandey, R. Comprehensive device simulation of 23.36% efficient two-terminal perovskite-PbS CQD tandem solar cell for low-cost applications. *Sci. Rep.* **2021**, *11*, 841. [CrossRef] [PubMed]

15. Lee, J.-W.; Kim, S.-G.; Yang, J.-M.; Yang, Y.; Park, N.-G. Verification and mitigation of ion migration in perovskite solar cells. *APL Mater.* **2019**, *7*, 041111. [CrossRef]

16. Zhou, Y.; Yang, M.; Pang, S.; Zhu, K.; Padture, A.N. Exceptional morphology-preserving evolution of formamidium lead triiodide perovskite thin films via organic-cation displacement. *J. Am. Chem. Soc.* **2016**, *138*, 5535. [CrossRef]

17. Wang, Y.; Zhang, G.; Li, G.; Xu, F.; Wang, T.; Li, Y.; Yang, Y.; Zhao, Y. A mixed-cation lead iodide $MA_{1-x}EA_xPbI_3$ absorber for perovskite solar cells. *J. Energy Chem.* **2018**, *27*, 125. [CrossRef]

18. Ueoka, N.; Oku, T.; Suzuki, A. Additive effects of alkali metals on Cu-modified $CH_3NH_3PbI_{3-\delta}Cl_\delta$ photovoltaic devices. *RSC Adv.* **2019**, *9*, 24231. [CrossRef]

19. Ferdani, W.D.; Pering, R.S.; Ghosh, D.; Kubiak, P.; Walker, B.A.; Lewis, E.S.; Johnson, L.A.; Baker, J.P.; Islam, S.M.; Cameron, J.P. Partial cation substitution reduces iodide ion transport in lead iodide perovskite solar cells. *Energy Environ. Sci.* **2019**, *12*, 2264. [CrossRef]

20. Ueoka, N.; Oku, T. Effects of co-addition of sodium chloride and copper(ii) bromide to mixed-cation mixed-halide perovskite photovoltaic devices. *ACS Appl. Energy Mater.* **2020**, *9*, 24231. [CrossRef]

21. Kandori, S.; Oku, T.; Nishi, K.; Kishimoto, T.; Ueoka, N.; Suzuki, A. Fabrication and characterization of potassium- and formamidinium-added perovskite solar cells. *J. Ceram. Soc. Jpn.* **2020**, *128*, 805. [CrossRef]

22. Ueoka, N.; Oku, T.; Suzuki, A. Effects of doping with Na, K, Rb, and formamidinium cations on $(CH_3NH_3)_{0.99}Rb_{0.01}Pb_{0.99}Cu_{0.01}I_{3-x}(Cl, Br)_x$ perovskite photovoltaic cells. *AIP Adv.* **2020**, *10*, 125023. [CrossRef]

23. Hoefler, F.S.; Trimmel, G.; Rash, T. Progress on lead-free metal halide perovskites for photovoltaic applications: A review. *Monatsu. Chem.* **2017**, *148*, 795. [CrossRef] [PubMed]

24. Zhang, W.; Xiong, J.; Li, J.; Daoud, A.W. Guanidinium induced phase separated perovskite layer for efficient and highly stable solar cells. *J. Mater. Chem. A* **2019**, *7*, 9486. [CrossRef]

25. Kishimoto, T.; Suzuki, A.; Ueoka, N.; Oku, T. Effects of guanidinium addition to $CH_3NH_3PbI_{3-x}Cl_x$ perovskite photovoltaic devices. *J. Ceram. Soc. Jpn.* **2019**, *127*, 491. [CrossRef]

26. Mahapata, A.; Runjhun, R.; Nawrocki, J.; Lewinski, J.; Kalam, A.; Kumar, P.; Trivedi, S.; Tavakoli, M.M.; Prochowicz, D.; Yadav, P. Elucidation of the role of guanidinium incorporation in single-crystalline MAPbI$_3$ perovskite on ion migration and activation energy. *Phys. Chem. Chem. Phys.* **2020**, *22*, 11467. [CrossRef]

27. Gao, L.; Li, X.; Lin, Y.; Fang, J.; Huang, S.; Spanopoulos, L.; Li, X.; Wang, Y.; Chen, L.; Yang, G.; et al. Incorporated guanidinium expands the $CH_3NH_3PbI_3$ lattice and enhances photovoltaic performance. *ACS Appl. Mater. Interfaces* **2020**, *12*, 43885. [CrossRef]

28. Hou, X.; Hu, Y.; Lin, H.; Mei, A.; Li, X.; Duan, M.; Zhang, G.; Rong, Y.; Han, H. Effect of guanidinium on mesoscopic perovskite solar cells. *J. Mater. Chem. A* **2017**, *5*, 73. [CrossRef]

29. Jodlowski, A.; Roldan-Carmona, C.; Grancini, G.; Salado, M.; Ralaiarisoa, M.; Ahmad, S.; Koch, N.; Camacho, L.; Miguel, G.; Nazeeruddin, M. Large guanidinium cation mixed with methylammonium in lead iodide perovskites for 19% efficient solar cells. *Nat. Energy* **2017**, *2*, 972. [CrossRef]

30. Zhao, W.; Yao, Z.; Yu, F.; Yang, D.; Liu, S. Alkali metal doping for improved $CH_3NH_3PbI_3$ perovskite solar cells. *Adv. Sci.* **2018**, *5*, 1700131. [CrossRef]

31. Li, N.; Luo, Y.; Chen, Z.; Niu, X.; Zhang, X.; Lu, J.; Kumar, R.; Jiang, J.; Liu, H.; Guo, X.; et al. Microscopic Degradation in Formamidinium-Cesium Lead Iodide Perovskite Solar Cells under Operational Stressors. *Joule* **2020**, *4*, 8. [CrossRef]

32. Lin, D.; Li, Q.; Wu, K. Ethylammonium as an alternative cation for efficient perovskite solar cells from first-principles calculations. *RSC Adv.* **2019**, *9*, 7356.

33. Nishi, K.; Oku, T.; Kishimoto, T.; Ueoka, N.; Suzuki, A. Photovoltaic Characteristics of $CH_3NH_3PbI_3$ Perovskite Solar Cells Added with Ethylammonium Bromide and Formamidinium Iodide. *Coatings* **2020**, *10*, 410. [CrossRef]

34. Solanki, A.; Yadav, P.; Turren-Cruz, S.-H.; Lim, S.S.; Saliba, M.; Sum, C.T. Cation influence on carrier dynamics in perovskite solar cells. *Nano Energy* **2019**, *58*, 604. [CrossRef]

35. Tyrren-Cruz, S.H.; Saliba, M.; Mayer, T.M.; Juarez-Santiesteban, H.; Mathew, X.; Nienhaus, L.; Tress, W.; Erodici, P.M.; Sher, M.-J.; Bawendi, G.M.; et al. Enhanced charge carrier mobility and lifetime suppress hysteresis and improve efficiency in planar perovskite solar cells. *Energy Environ. Sci.* **2018**, *11*, 78. [CrossRef]

36. Cui, S.; Wang, J.; Xie, H.; Zhao, Y.; Li, Z.; Luo, S.; Ke, L.; Gao, Y.; Meng, K.; Ding, L.; et al. Rubidium Ions Enhanced Crystallinity for Ruddlesden–Popper Perovskites. *Adv. Sci.* **2020**, *7*, 2002445. [CrossRef]

37. Oku, T.; Kandori, S.; Taguchi, M.; Suzuki, A.; Okita, M.; Minami, S.; Fukunishi, S.; Tachikawa, T. Polysilane-inserted methylammonium lead iodide perovskite solar cells doped with formamidinium and potassium. *Energies* **2020**, *13*, 4776. [CrossRef]

38. Han, T.-H.; Lee, J.-W.; Choi, C.; Tan, S.; Lee, C.; Zhao, Y.; Dai, Z.; Marco, D.N.; Lee, S.J.; Bae, S.H.; et al. Perovskite-polymer composite cross-linker approach for highly-stable and efficient perovskite solar cells. *Nat. Commun.* **2019**, *10*, 520. [CrossRef]

39. Taguchi, M.; Suzuki, A.; Ueoka, N.; Oku, T. Effects of poly(methyl methacrylate) addition to perovskite photovoltaic devices. *AIP Conf. Proc.* **2019**, *2067*, 020018. [CrossRef]

40. Oku, T.; Nakagawa, J.; Iwase, M.; Kawashima, M. Microstructures and photovoltaic properties of polysilane-based solar cells. *Jpn. J. Appl. Phys.* **2013**, *52*, 04CR07. [CrossRef]

41. Taguchi, M.; Suzuki, A.; Oku, T.; Ueoka, N.; Minami, S.; Okita, M. Effects of annealing temperature on decaphenylcyclopentasilane-inserted $CH_3NH_3PbI_3$ perovskite solar cells. *Chem. Phys. Lett.* **2019**, *737*, 136822. [CrossRef]

42. Oku, T.; Taguchi, M.; Suzuki, A.; Kitagawa, K.; Asakawa, Y.; Yoshida, S.; Okita, M.; Minami, S.; Fukunishi, S. Effects of polysilane addition to chlorobenzene and high temperature annealing on $CH_3NH_3PbI_3$ perovskite photovoltaic devices. *Coatings* **2021**, *11*, 665. [CrossRef]

43. Oku, T.; Ohishi, Y.; Ueoka, N. Highly (100)-oriented $CH_3NH_3PbI_3$(Cl) perovskite solar cells prepared with NH_4Cl using an air blow method. *RSC Adv.* **2018**, *8*, 10389–10395. [CrossRef]

44. Stranks, D.S.; Eperon, E.G.; Grancini, G.; Menelaou, C.; Alcocer, P.J.M.; Leijtens, T.; Herz, M.L.; Petrozza, A.; Snaith, J.H. Electron-hole diffusion lengths exceeding 1 micrometer in an organometal trihalide perovskite absorber. *Science* **2013**, *342*, 341. [CrossRef]

45. Dong, Q.; Fang, Y.; Shao, Y.; Mulligan, P.; Qiu, J.; Cao, L.; Huang, J. Electron-hole diffusion lengths > 175 μm in solution-grown $CH_3NH_3PbI_3$ single crystals. *Science* **2015**, *347*, 967. [CrossRef]

46. Oku, T.; Zushi, M.; Imanishi, Y.; Suzuki, A.; Suzuki, K. Microstructures and photovoltaic properties of perovskite-type $CH_3NH_3PbI_3$ compounds. *Appl. Phys. Express* **2014**, *7*, 121601. [CrossRef]

47. Ueoka, N.; Oku, T. Stability characterization of PbI_2-added $CH_3NH_3PbI_{3-x}Cl_x$ photovoltaic devices. *ACS Appl. Mater. Interfaces* **2018**, *10*, 44443–44451. [CrossRef]

48. Oku, T. Crystal structures of perovskite halide compounds used for solar cells. *Rev. Adv. Mater. Sci.* **2020**, *59*, 264–305. [CrossRef]

49. Suzuki, A.; Kishimoto, K.; Oku, T.; Okita, M.; Fukunishi, S. Tachikawa, Additive effect of lanthanide compounds into perovskite layer on photovoltaic properties and electronic structures. *Synth. Met.* **2022**, *287*, 117092. [CrossRef]

50. Kishimoto, T.; Oku, T.; Suzuki, A.; Ueoka, N. Additive effects of guanidinium iodide on $CH_3NH_3PbI_3$ perovskite solar cells. *Phys. Status Solidi A* **2021**, *218*, 2100396. [CrossRef]

51. Enomoto, A.; Suzuki, A.; Oku, T.; Okita, M.; Fukunishi, S.; Tachikawa, T.; Hasegawa, T. Effects of Cu, K and guanidinium addition to $CH_3NH_3PbI_3$ perovskite solar cells. *J. Electron. Mater.* **2022**. [CrossRef]

52. Suzuki, A.; Taguchi, M.; Oku, T.; Okita, M.; Minami, S.; Fukunishi, S.; Tachikawa, T. Additive effects of methyl ammonium bromide or formamidinium bromide in methylammonium lead iodide perovskite solar cells using decaphenylcyclopentasilane. *J. Mater. Sci. Mater. Electron.* **2021**, *32*, 26449–26464. [CrossRef]

53. Suzuki, A.; Oku, T. Electronic structures and magnetic properties of transition metal doped $CsPbI_3$ perovskite compounds by first-principles calculation. *Phys. Solid State* **2019**, *61*, 1074–1085. [CrossRef]

54. Suzuki, A.; Oe, M.; Oku, T. Fabrication and characterization of Ni-, Co-, and Rb-incorporated $CH_3NH_3PbI_3$ perovskite solar cells. *J. Electronic Mater.* **2021**, *50*, 1980–1995. [CrossRef]

55. Suzuki, A.; Kitagawa, K.; Oku, T.; Okita, M.; Fukunishi, S.; Tachikawa, T. Additive effects of copper and alkali metal halides into methylammonium lead iodide perovskite solar cells. *Electron. Mater. Lett.* **2022**, *18*, 176–186. [CrossRef]

56. Suzuki, A.; Oku, T. Effects of mixed-valence states of Eu-doped $FAPbI_3$ perovskite crystals studied by first-principles calculation. *Mater. Adv.* **2021**, *2*, 2609–2616. [CrossRef]

57. Suzuki, A.; Oku, T. First-principles calculation study of electronic structures of alkali metals (Li, K, Na and Rb)-incorporated formamidinium lead halide perovskite compounds. *Appl. Surf. Sci.* **2019**, *483*, 912–921. [CrossRef]

58. Suzuki, A.; Oku, T. Effects of transition metals incorporated into perovskite crystals on the electronic structures and magnetic properties by first-principles calculation. *Heliyon* **2018**, *4*, e00755. [CrossRef]

59. Okumura, R.; Oku, T.; Suzuki, A.; Okita, M.; Fukunishi, S.; Tachikawa, T.; Hasegawa, T. Effects of adding alkali metals and organic cations to Cu-based perovskite solar cells. *Appl. Sci.* **2022**, *12*, 1710. [CrossRef]
60. Ono, I.; Oku, T.; Suzuki, A.; Asakawa, Y.; Terada, S.; Okita, M.; Fukunishi, S.; Tachikawa, T. Fabrication and characterization of $CH_3NH_3PbI_3$ solar cells with added guanidinium and inserted with decaphenylpentasilane. *Jpn. J. Appl. Phys.* **2022**, *61*, SB1024. [CrossRef]